MIT Libraries | DSpace@MIT

MIT Open Access Articles

Axisymmetric reflectors in wave energy converter arrays: Harnessing scattering to increase energy extraction

Massachusetts Institute of Technology

Axisymmetric reflectors in wave energy converter arrays: Harnessing scattering to increase energy extraction ⊖

Grgur Tokić ✉ ⓘ ; Dick K. P. Yue ⓘ

Check for updates
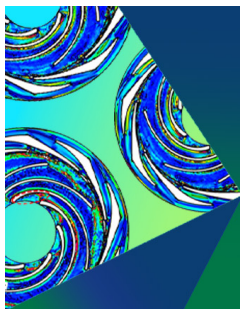
View Online   Export Citation   CrossMark

Axisymmetric reflectors in wave energy converter arrays: Harnessing scattering to increase energy extraction 🄴🄿

View Online   Export Citation   CrossMark

Grgur Tokić[a] 🄸🄳 and Dick K. P. Yue[b] 🄸🄳

AFFILIATIONS

Department of Mechanical Engineering, Massachusetts Institute of Technology, Cambridge, Massachusetts 02139, USA

Note: This paper is part of the special topic, Recent Advances in Marine Hydrodynamics.
[a] Author to whom correspondence should be addressed: gtokic@mit.edu
[b] yue@mit.edu

ABSTRACT

We elucidate the effect of non-extracting reflectors on the performance of wave energy converter (WEC) arrays. We consider an infinitely periodic row of converters parallel to an infinitely periodic row of discrete axisymmetric reflectors (C-R arrays), and we study how the spatial configuration affects energy extraction. Using a multiple-scattering algorithm for linear wave-array interactions, we conduct a series of simulations of C-R arrays for a range of spatial configuration parameters, wavenumbers, and wave incident angles. We find that C-R arrays can significantly increase energy extraction compared to a WEC array by itself. We offer a simplified theoretical model, based on the far-field response of periodic rows in isolation, which shows that the large increases in energy extraction result from the constructive Bragg and Laue interferences caused by wave interactions with the reflector row. For the pertinent case of incident waves of the WEC-resonant frequency, we find that optimized C-R arrays can achieve energy extraction gains of $O(500\%)$. Remarkably, the optimal C-R array extracts more energy than two rows of converters of optimal configuration even though the C-R array consists of only half as many WECs.

I. INTRODUCTION

Wave energy converter (WEC) arrays present a promising technological solution for large-scale wave energy extraction. This is in large part due to their ability to harness favorable wave interactions occurring within the array to extract more energy than what the same number of converters in isolation would extract.[1,2] In recent years, with the impetus to move wind farms further offshore, there are incentives to co-locate WEC arrays with these structures in order to share logistics and infrastructure. While the economic and operational benefits are established,[3,4] the physics-based synergisms between wave and wind farms have not been well studied. One such synergism is the possibility to harness the wave reflections from wind turbine platforms to increase the energy extraction of the WEC array in its vicinity through favorable wave interactions. Motivated by this, our interest here is the physical mechanisms and magnitudes of possible wave energy extraction gains achieved by WEC arrays when operated in the vicinity of other structures that consist of a large number of immersed, vertical, axisymmetric elements.

Harnessing wave reflections is a well known approach to increase energy extraction. In solar cells, for example, a backing mirror can double the absorption of a semiconducting parallel slab by effectively doubling its thickness, but much larger enhancements can be achieved if the mirror is combined with random or periodic structures on the surface of the semiconductor that further reflect waves.[5,6] In WEC arrays, an infinite vertical wall, such as a breakwater or a coastal cliff face, can play a role of a mirror. Recently, hydrodynamic studies of small WEC arrays (five bodies) in a limited number of configurations in front of an infinite reflecting wall[7,8] showed that the energy extraction gain can be significant. Similarly, an infinitely periodic row of scatterers generally also reflects incident waves, so it could, in principle, lead to an increase in energy extraction of a WEC array placed in its vicinity. Compared to using a reflecting mirror, however, employing a periodic row of scatterers as the reflecting structure leads to a more complex performance, since the scattering characteristics of the row are dependent on the incident wavenumber, the reflector type, and their spatial configuration (periodicity). Furthermore, for

20 November 2023 20:14:23

sufficiently large wavenumbers, more than one reflected and transmitted modes are present.[9,10] In the water wave context, wave interactions in infinitely periodic arrays of general scatterers[11,12] or identical WECs[13–17] have been studied; heterogeneous arrays consisting of a small, finite number of different WECs have also been studied.[18] Wave interactions in hybrid WEC-reflector arrays, however, have not been studied to date.

In this study, we investigate the energy extraction performance of WEC arrays co-located with arrays of axisymmetric reflectors. For simplicity and specificity, we focus on arrays that consist of a single infinitely periodic row of WECs in the vicinity of (and parallel to) a single infinitely periodic row of reflectors. We denote these as C-R arrays. We consider reflectors (R) to have the same geometry as converters (C), but whose overall scattering response is different due to the different motion constraints, and consider different scenarios where the reflector is fixed, freely heaving, or even extracting energy. We contrast the behavior of such C-R arrays to that of isolated WEC arrays consisting of a single periodic row of converters with a goal to understand the fundamental underlying physical mechanisms of the reflector-caused energy extraction gain and the required conditions for it.

In Sec. II, we define in detail the converters, reflectors, and the array configurations that we study. In Sec. III, we give a brief overview of the linear multiple-scattering mathematical model that we employ.[17] We conduct systematic computations of wave–array interactions to quantify the energy extraction performance of C-R arrays as a function of spatial configuration (Sec. IV). We find that optimized C-R array configurations can extract significantly more energy, by as much as $O(250\%)$ over optimized isolated periodic WEC arrays, and as much as $O(500\%)$ compared to WECs operating in isolation. We offer a simplified theoretical model based on plane wave scattering (Sec. V), which explains the underlying mechanisms responsible for the extrema in energy extraction. The comparisons among C-R arrays consisting of different reflector types and those of different periodicities of the two rows are presented in Sec. VI. We show that increasing the reflector strength, by either changing its type or increasing their number relative to that of converters, further increases the energy extraction of C-R arrays.

II. PROBLEM DEFINITION

We study the hydrodynamic and energetic response of C-R arrays in water of uniform depth h. A row of converters (C) and a row of reflectors (R) are both periodic and parallel to each other, Fig. 1.

For simplicity, we consider identical WEC and reflector body geometries.

We consider WECs oscillating in heave (only), connected to a power takeoff (PTO) device with a linear force-velocity characteristic β (extraction rate). The power extracted by the PTO is linearly proportional to β. Specifically, we set the extraction rate $\beta = \beta^*$ for all WECs, where $\beta^* = b(k_r)$ is the optimal PTO extraction rate, which is equal to the radiation damping b at the body resonant wavenumber k_r. The power P_0 extracted by an isolated WEC with $\beta = \beta^*$ is such that the capture width $W \equiv P_0/\mathcal{P}$ achieves the theoretical maximum $k_r W = 1$ for monochromatic incident waves of wavenumber $k = k_r$;[19] here, $\mathcal{P} \equiv 1/2\rho g A^2 c_g$ is the wave energy flux per unit length of wavefront carried by the incident wave of amplitude A and group velocity c_g.

We consider three types of reflectors, distinguished by their motion constraint—freely heaving reflectors (F), fixed reflectors (X), and reflectors that are themselves converters (C). The reflector motion constraint can be thought of as reflectors being connected to PTOs with different β values—$\beta = 0$ for F-reflectors; $\beta \to \infty$ for X-reflectors; and $\beta = \beta^*$ for C-reflectors. In this study, we consider the WEC and reflector geometry to be that of a truncated vertical cylinder of radius $a/h = 0.3$ and draft $H/h = 0.2$. The wavenumber-dependent performance of this truncated vertical cylinder operating in isolation as a WEC (C), as a freely oscillating body (F), and as a fixed body (X) is given in Fig. 2.

To quantify the scattering strength of isolated devices, particularly when acting as reflectors, we define a total scattering cross section σ. Analogously to the capture width, the scattering cross section of an isolated scatterer can be interpreted as the equivalent crest-wise length of a vertical wall that perfectly reflects the same amount of incident wave energy as that scattered by the body into the far field.[20] Traditionally, σ is obtained for the diffraction problem only,[21,22] and it is a wavenumber-dependent characteristic of a body's shape, not its potential motion. Here, we generalize σ to also account for the energy carried to the far field by the waves radiated due to the body motion (defined in mathematical terms in Sec. III). With this generalized definition, σ of C, F, and X bodies is different, despite them having the same geometry, Fig. 2(b). As the resonant wavenumber k_r is such that $k_r a = O(1)$ for our geometry, the scattering at k_r is strong, $\sigma/2a = O(1)$, for all reflector types, Fig. 2(b).
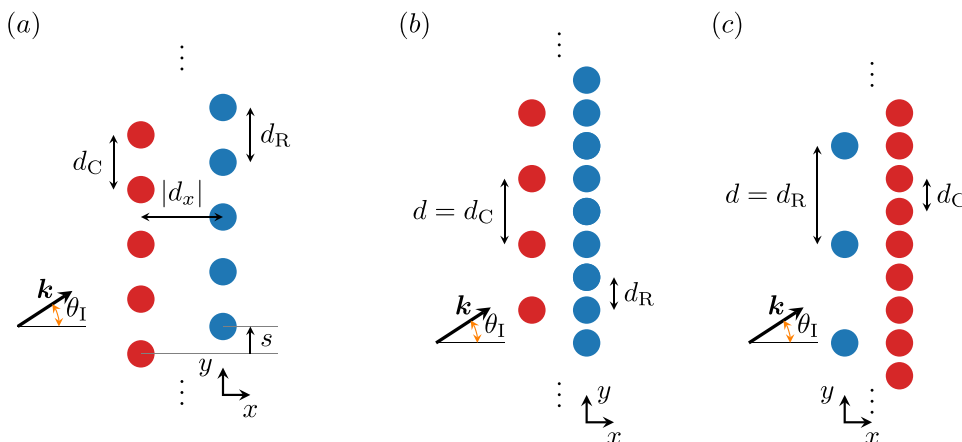
FIG. 1. Select spatial configurations of C-R arrays [(red filled circle) = WEC; (blue filled circle) = reflector]. (a) C → R array with non-zero row shift $s \neq 0$ and reflector periodicity factor $\nu = d_C/d_R = 1$; array periodicity $d = d_C = d_R$. Number of bodies per periodic cell $N = 2$, number of WECs per periodic cell $N_C = 1$, number of reflectors per periodic cell $N_R = 1$. (b) C → R array with $s = 0$ and $\nu = 2$; $N = 3$, $N_C = 1$, $N_R = 2$. (c) R → C array with $s = 0$ and $\nu = 1/3$; $N = 4$, $N_C = 3$, $N_R = 1$.
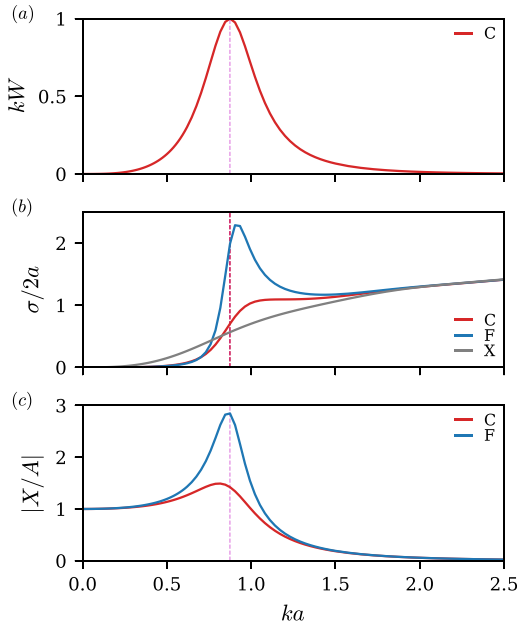
FIG. 2. Performance of an isolated truncated cylinder (radius $a/h = 0.3$, draft $H/h = 0.2$) operating as a WEC (C), a freely oscillating body (F), and a fixed body (X). The vertical dashed line marks the body resonant wavenumber k_r. (a) Non-dimensional capture width kW; (b) total scattering cross section σ; (c) heave amplitude $|X|$.

Depending on the type of reflectors (R = F, X, or C), we denote C-R arrays as C-F, C-X, and C-C arrays, respectively. Where needed, to distinguish the order of the two rows relative to the incident wave, we also use the notations R → C (and C → R) for an array with the R-row in front of (behind) the C-row. We use S-array to denote a single-row periodic array and use the notation $\mathcal{S}_F$, $\mathcal{S}_X$, or $\mathcal{S}_C$ to indicate its constituent body type.

We focus on C-R arrays of periodicity d and inter-row spacing d_x, Fig. 1. We define d_x relative to the R-row, with $d_x > 0$ for R → C arrays and $d_x < 0$ for C → R arrays. In general, there can be a non-zero shift s between the two rows in the span-wise (y) direction. In a C-R array, the periodicity of the WEC row is d_C and that of the reflector row is d_R. The periodicities can be equal $d_C = d_R = d$, or, in the more general case, $\nu \equiv d_C/d_R \neq 1$. For the overall C-R array to be periodic, the reflector periodicity factor ν must be a rational number, with the resulting periodicity d of the C-R array being the lowest common multiple of d_C and d_R. The reflector periodicity factor can then also be expressed as $\nu = N_R/N_C$, where N_R and N_C are the resulting numbers of reflectors and WECs within a periodic cell of periodicity d, respectively. The total number of bodies in a periodic cell of a C-R array is $N = N_C + N_R \geq 2$; if $\nu = 1$, $N = 2$. In this study, we only consider C-R arrays where either N_C or N_R is equal to one.

A measure of energy extraction efficacy of a general WEC array is the array gain q,

$$q = \frac{P}{N_C \times P_0}, \qquad (1)$$

the ratio between the power P extracted by the array consisting of N_C WECs and the power P_0 extracted by a single WEC operating in

isolation.[1] This array gain quantifies the increase in energy extraction due to wave interactions among the bodies in the array, and it is strongly dependent on the spatial array configuration. This definition of array gain also applies for C-R arrays, where it quantifies the gain in energy extraction per periodic cell, with N_C being the number of converters in a periodic cell. In the special case of C-C arrays with $\nu = 1$, for example, the total extracted power P per periodic cell comes from twice as many WECs ($N_C = 2$) as in C-F or C-X ($N_C = 1$) arrays. The array gain of different C-R array configurations is differentiated by a subscript corresponding to the reflector type, e.g., q_R for C-R arrays in general, q_F for C-F arrays. Among S-arrays ($N = 1$), only $\mathcal{S}_C$ arrays are energy extracting ($N = N_C = 1$), and we denote their gain as q_S.

Note that the incident energy flux per periodic cell $\mathcal{P}d \cos \theta_I$ is finite in infinitely periodic arrays, so it is theoretically possible to extract 100% of it. For periodic arrays consisting only of axisymmetric heaving WECs, 100% extraction requires $N_C > 1$, as the optimal $\mathcal{S}_C$-array can only extract 50% of the incident energy flux.[13,17] However, while the total extracted energy generally increases with increasing N_C, it can come with diminishing returns per additional WEC, resulting in a lower array gain. In fact, the maximum obtainable gain of arrays consisting of N_C infinitely periodic rows of optimal heaving WECs diminishes with $1/N_C$.[17]

We also note that the PTO extraction rate $\beta = \beta^*$, while optimal for a WEC in isolation, is not, in general, optimal for the same WECs operating as a part of an array. In WEC arrays, the optimal β is, in general, different for every WEC in an array (or within a periodic cell), and it is dependent on the spatial array configuration. For simplicity and consistency, we keep $\beta = \beta^*$ for WECs in all array configurations. We particularly focus on body resonant wavenumber k_r in Secs. IV and VI to showcase the efficacy of wave interaction-caused energy extraction gain q over the already best-case-scenario, optimal performance of isolated WECs. Consequently, the obtained values of q_R in Secs. IV and VI could be larger if β of WECs were set to configuration-dependent optimal values.

III. MATHEMATICAL MODEL

We apply an exact multiple scattering wave-body interaction model in the context of linearized potential theory. This method was introduced in Ref. 23 and expanded for periodic arrays of general bodies in Ref. 17. For completeness, we summarize it here for the present application.

We consider linear incident waves of angular frequency ω, wavenumber k, amplitude A ($kA \ll 1$, dispersion relation $\omega^2 = gk\tanh kh$), and incident angle θ_I. We consider a three-dimensional, time-harmonic potential $\Phi = \text{Re}(\phi\, e^{-i\omega t})$, where ϕ is the time-independent, complex-valued potential and i is the imaginary unit. For linear wave–multi-body interactions, the potential ϕ can be expressed as

$$\phi = \phi^I + \sum_j \left(\phi_j^S + V_j \phi_j^R \right) = \phi_p^I + \phi_p^S + V_p \phi_p^R, \qquad (2)$$

where ϕ^I is the ambient incident wave potential, $\sum_j$ is the summation over all bodies in the array, and ϕ_j^S and ϕ_j^R are the scattered and unit-velocity radiated wave potentials associated with body $\mathcal{B}_j$, respectively. The complex heave velocity amplitude of $\mathcal{B}_j$ is V_j; if $\mathcal{B}_j$ is fixed, $V_j = 0$. Focusing on a particular body $\mathcal{B}_p$, ϕ can be further rewritten in terms of the total incident wave potential ϕ_p^I on $\mathcal{B}_p$, where ϕ_p^I is the sum of the ambient incident wave on $\mathcal{B}_p$ and the scattered and radiated waves

20 November 2023 20:14:23

from other bodies $\mathcal{B}_j$, $j \neq p$. The boundary conditions applied on the wetted surface $\mathscr{S}_p$ of every body $\mathcal{B}_p$ in the array are

$$\frac{\partial \phi_p^I}{\partial n} = -\frac{\partial \phi_p^S}{\partial n}, \quad \boldsymbol{x} \in \mathscr{S}_p, \forall p, \tag{3}$$

$$\frac{\partial \phi_p^R}{\partial n} = n_z, \quad \boldsymbol{x} \in \mathscr{S}_p, \forall p. \tag{4}$$

In (4), n_z is the vertical component of the unit normal on $\mathscr{S}_p$.

In order to separate the individual body hydrodynamic response from the array-related hydrodynamic interactions, we restrict the potential ϕ to be defined in the fluid domain $\mathscr{D} = \mathscr{D}_0 \setminus \cup_p \mathscr{D}_p$. Here, $\mathscr{D}_0$ is the infinite domain bounded by the bottom and the free surface, and $\mathscr{D}_p$ is the finite fluid domain beneath each body $\mathcal{B}_p$ in the array, Fig. 3(a). The governing equation for ϕ in $\mathscr{D}$ is the Helmholtz equation $\partial_x^2 \phi + \partial_y^2 \phi \pm \kappa^2 \phi = 0$, where the plus sign corresponds to the propagating wave solution, with $\kappa \equiv k$; and the minus sign corresponds to the evanescent wave solutions, where $\kappa \equiv k_m$, $m > 0$ satisfy the evanescent wave dispersion relation $\omega^2 = -g k_m \tan k_m h$.

In the cylindrical coordinate system (r_p, ϑ_p, z) centered at $\mathcal{B}_p$, Fig. 3(b), the potentials in (2) can be expanded into partial waves as

$$
\begin{aligned}
\phi_p^I &= \sum_{m=0}^{\infty} \sum_{n=-\infty}^{\infty} d_{m,n}^p \mathrm{I}_n(k_m r_p) e^{in\vartheta_p} \psi_m(z), \\
\phi_p^S &= \sum_{m=0}^{\infty} \sum_{n=-\infty}^{\infty} c_{m,n}^p \mathrm{K}_n(k_m r_p) e^{in\vartheta_p} \psi_m(z), \\
\phi_p^R &= \sum_{m=0}^{\infty} \sum_{n=-\infty}^{\infty} \varrho_{m,n}^p \mathrm{K}_n(k_m r_p) e^{in\vartheta_p} \psi_m(z),
\end{aligned}
\tag{5}
$$

where $d_{m,n}^p$, $c_{m,n}^p$, and $\varrho_{m,n}^p$ are the complex partial wave amplitudes. Here, I_n and K_n are modified Bessel functions of the first and the second kind, respectively; $\psi_m(z)$ is the orthonormal depth function. To facilitate expressing both propagating $(m = 0)$ and evanescent $(m > 0)$ partial waves with the same functions in Eq. (5), we define $k_0 \equiv -ik$ and use the well-known identities $\mathrm{K}_n(-ik) = \frac{\pi}{2} i^{n+1} \mathrm{H}_n^{(1)}(k)$ and $\mathrm{I}_n(-ik) = i^{-n} \mathrm{J}_n(k)$.[24] Here, $\mathrm{H}_n^{(1)}$ is the Hankel function of the first kind, which describes the outwardly propagating waves, and J_n is the Bessel function of the first kind.
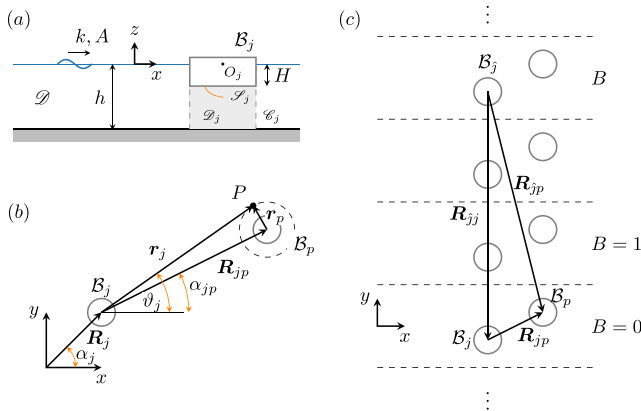
FIG. 3. (a) Side view of the domain; incident wave of amplitude A, wavenumber k. (b) Coordinate systems and the relative position vector $\boldsymbol{R}_{jp}$ decomposition for two bodies $\mathcal{B}_j$ and $\mathcal{B}_p$ within the same periodic cell. (b) Decomposition of the relative position vector $\boldsymbol{R}_{jp}$ for bodies $\mathcal{B}_j$ and $\mathcal{B}_p$, which are in different periodic cells.

The partial amplitudes $c_{m,n}^p$ and $d_{m,n}^p$ depend on the array configuration $\mathcal{C}$ and need to be solved for. The unit-velocity radiated partial wave amplitudes $\varrho_{m,n}^p$ are known, as determined from the radiation problem for $\mathcal{B}_p$ in isolation (the heave velocity V_p is unknown). We use $\varrho_{m,n}^p$ from an analytic solution[25] for ϕ_p^R of a heaving truncated cylinder in $\mathscr{D}_0 \setminus \mathscr{D}_p$. The incident partial wave amplitudes $d_{m,n}^p$ are the sum of the known incident ambient partial wave amplitude

$$d_{m,n}^{I,p} = (-1)^n e^{ikR_p \cos(\theta_I - \alpha_p)} e^{-in\theta_I} \tag{6}$$

at $\mathcal{B}_p$ and the contributions of the scattered and radiated waves $c_{m,n}^j$ of bodies $\mathcal{B}_j$ expressed in the $\mathcal{B}_p$ coordinate system. For compactness, we collect $d_{m,n}^p$, $d_{m,n}^{I,p}$, $c_{m,n}^p$, and $\varrho_{m,n}^p$ into vector forms $\boldsymbol{d}_p$, $\boldsymbol{d}_p^I$, $\boldsymbol{c}_p$, and $\boldsymbol{\varrho}_p$, respectively.

The equation of motion of a non-fixed body $\mathcal{B}_p$, expressed in terms of the complex heave amplitude X_p, is

$$\mathbf{A}_p(\omega) \cdot \boldsymbol{X}_p = \boldsymbol{F}_p(\omega, \mathcal{C}), \tag{7}$$

where $\mathbf{A}_p$ is the conventional, frequency-dependent body dynamics matrix,[17,21] and $\boldsymbol{F}_p(\omega, \mathcal{C})$ is the configuration-dependent diffraction force on $\mathcal{B}_p$; the size of the linear system equals the number of degrees of freedom of $\mathcal{B}_p$. The diffraction force can be expressed in terms of the amplitudes of the scattered waves as $\boldsymbol{F}_p(\omega, \mathcal{C}) = \hat{\mathbf{F}}_p^T \cdot \boldsymbol{c}_p$, where $\hat{\mathbf{F}}_p(\omega)$ is the diffraction force transfer matrix known from the diffraction problem of isolated $\mathcal{B}_p$ [$(\cdot)^T$ denotes a matrix transpose]. The amplitude of the radiated waves due to the velocity amplitude $V_p = -i\omega X_p$ can be expressed in terms of the scattered wave amplitudes $\boldsymbol{c}_p$ as $\boldsymbol{\varrho}_p \cdot V_p = \mathbf{H}_p \cdot \boldsymbol{c}_p$, where $\mathbf{H}_p(\omega) = -i\omega \boldsymbol{\varrho}_p \mathbf{A}_p^{-1} \hat{\mathbf{F}}_p^T$ is the radiation transfer matrix of $\mathcal{B}_p$, which can be calculated for a body in isolation. In addition to frequency, $\mathbf{H}_p$ depends only on the body shape and its PTO, and it is non-zero only if $\mathcal{B}_p$ is free to oscillate. For the present problem, we only consider bodies oscillating in heave, so $\mathbf{A}_p$, X_p, V_p, and $\boldsymbol{F}_p$ reduce to scalars and $\hat{\mathbf{F}}_p$ to a vector. Due to the differences in PTO connection, β contained in $\mathbf{A}_p$, $\mathbf{H}_p$ is different for C, F, and X bodies. As the body geometries considered here are truncated vertical cylinders, we use analytical expressions for hydrodynamic quantities related to the performance of bodies in isolation—from Ref. 25 for added mass and radiation damping that are contained in $\mathbf{A}_p$ and from Ref. 26 for $\hat{\mathbf{F}}_p$.

The partial wave amplitudes $\boldsymbol{c}_p$ and $\boldsymbol{d}_p$ for every $\mathcal{B}_p$ in the array are related through the diffraction boundary condition (3). The relationship can be expressed in terms of a linear system $\boldsymbol{c}_p = \mathbf{T}_p \cdot \boldsymbol{d}_p$, where the frequency-dependent scattering transfer matrix $\mathbf{T}_p(\omega)$ has to be obtained from the diffraction problem on an isolated body for each body geometry type.[27] As all bodies in the present problem are truncated cylinders, we use an analytical solution for the scattered wave amplitudes.[26]

Enforcing the diffraction boundary condition on every $\mathcal{B}_p$ in the array leads to a linear system for the unknown amplitudes $\boldsymbol{c}_p$, $p = 1, \ldots, N$,

$$\sum_{j=1}^N \left[\delta_{jp} - \mathbf{T}_j \big((1 - \delta_{jp}) \mathbf{S}_{jp} + \mathbf{Q}_{jp} \big)^T (\mathbf{I} + \mathbf{H}_j) \right] \boldsymbol{c}_j = \mathbf{T}_p \boldsymbol{d}_p^I. \tag{8}$$

Here, N is the number of bodies in a periodic cell, δ_{jp} is the Kronecker delta, and $\mathbf{I}$ is the identity matrix. The effect of array configuration is

expressed through matrices $\mathbf{S}_{jp}$ and $\mathbf{Q}_{jp}$. The separation matrix $\mathbf{S}_{jp}$ depends only on the relative positions of the bodies in the array, and it arises from expressing ϕ_j^S in the coordinate system of $\mathcal{B}_p$ through the Graf addition theorem[27]

$$K_n(k_m r_j)e^{in\vartheta_j} = \sum_{l=-\infty}^{\infty} S_{m,n,l}^{jp} I_l(k_m r_p) e^{il\vartheta_p}, \quad r_p < R_{jp}. \quad (9)$$

Here, $S_{m,n,l}^{jp} = (-1)^l K_{n-l}(k_m R_{jp}) e^{i(n-l)\alpha_{jp}}$ are the elements of $\mathbf{S}_{jp}$; R_{jp} is the distance between bodies $\mathcal{B}_j$ and $\mathcal{B}_p$, and α_{jp} is the angle between them, Fig. 3(b). Similarly, the periodicity matrix $\mathbf{Q}_{jp}$ encodes the equivalent coordinate system transformations between bodies $\mathcal{B}_j$ and $\mathcal{B}_p$ in different periodic cells, Fig. 3(c), with elements[17]

$$Q_{m,n,l}^{jp} = (-1)^l \sum_{\substack{B=-\infty, \\ B \neq 0}}^{\infty} K_{n-l}(k_m R_{jp})e^{i(n-l)\alpha_{jp}} e^{ikd\sin\theta_I}. \quad (10)$$

The method we use to calculate the infinite sums over all periodic cells in $Q_{m,n,l}^{jp}$ is given in the Appendix.

To solve (8), we limit the order of partial waves to $|n| \leq N_p$, and truncate the number of evanescent waves to $m \leq M$. The resulting linear system (8) is of size $NM_t \times NM_t$, where $M_t = (2N_p + 1)(M+1)$, and the vectors $\boldsymbol{c}_p, \boldsymbol{d}_p^I$ are of length M_t. Except for the error introduced by the truncation, the solution to system (8) is, in principle, exact in the context of the linearized potential flow. We truncate the partial wave decompositions to $N_p = 5$ and $M = 2$, which give converged results for the analyses presented in this study [error $o(10^{-2})$]. As a further check, we compare our results for select configurations of infinitely periodic arrays with the results for large, but finite arrays of equivalent configurations (consisting of 20 cells).

The power extracted by a body $\mathcal{B}_j$ oscillating with X_j can be calculated as

$$P_j = 1/2\beta\omega^2|X_j|^2 = \boldsymbol{c}_j^+ \Omega_j \boldsymbol{c}_j, \quad (11)$$

where Ω_j is the PTO-dependent, real, symmetric power transfer matrix

$$\Omega_j = 1/2\beta\omega^2 \hat{\mathbf{F}}_j (\mathbf{A}_j^{-1})^+ \mathbf{A}_j^{-1} \hat{\mathbf{F}}_j^+ \quad (12)$$

of $\mathcal{B}_j$ [$(\cdot)^+$ denotes a Hermitian transpose]. If a body is fixed or freely oscillating, $P_j = 0$. The total extracted power by an array is $P = \sum_{j=1}^{N} P_j$.

The free surface far away from a periodic array can be expressed solely in terms of outwardly propagating scattered plane waves (or modes). The transmitted modes, complex amplitude A_m^+, propagate at an angle θ_m, $|\theta_m| \leq \pi/2$, while the reflected modes, complex amplitude A_m^-, propagate at angle $\pi - \theta_m$. The propagation angle θ_m is determined from the diffraction grating equation[28]

$$\sin\theta_m = \sin\theta_I + m\frac{2\pi}{kd}, \quad m \in \mathcal{M}, \quad (13)$$

where $\mathcal{M}(\theta_I, kd) = \{m : |\sin\theta_m| \leq 1, m \in \mathbb{Z}\}$ is the set of all indices of the propagating modes in the far field. For an array with periodicity d, the critical wavenumbers $(kd)_m^{cr}$ at which new modes appear (known as Rayleigh wavenumbers) are given by $|\sin\theta_I + 2\pi m/(kd)_m^{cr}| = 1$. The complex amplitudes $A_m^\pm$ are given by[17]

$$A_m^\pm = \mp\frac{\omega\pi}{g} \frac{1}{kd} \frac{1}{\cos\theta_m} \sum_{j=1}^{N} e^{\mp ikR_j\cos(\theta_m \mp \alpha_j)}$$

$$\times \sum_{n=-\infty}^{\infty} (\pm 1)^n c_{0,n}^j e^{\pm in\theta_m}, \quad m \in \mathcal{M}. \quad (14)$$

The amplitudes are related through the energy conservation equation

$$\sum_{m\in\mathcal{M}} \left(|\delta_{0m} + A_m^+|^2 + |A_m^-|^2\right)\cos\theta_m = \cos\theta_I - \Delta, \quad (15)$$

where $\Delta \equiv P/(\mathcal{P} \times d) \leq \cos\theta_I$ accounts for the total power P extracted by all the converters in the array; δ_{0m} is the Kronecker delta function. At $(kd)_m^{cr}$, the wave energy is redistributed among the scattered modes, resulting in an abrupt change in the behavior of bodies in the array. This behavior is a manifestation of Rayleigh resonances.[17,29,30] The energy conservation check (15) is performed in all our calculations, and it is satisfied to $o(10^{-8})$.

The total scattering cross section σ of an isolated body is defined as

$$\mathcal{P} \times \sigma = -1/2\rho\omega \operatorname{Im} \iint_{S_\infty} \phi^o \frac{\partial\phi^{o*}}{\partial r} dS, \quad (16)$$

where the right-hand side represents the energy carried by the outwardly propagating waves through a virtual cylindrical surface S_∞ in the far field $(r \to \infty)$; the potential of these waves is $\phi^o = \phi^S + V\phi^R$. The free surface amplitude of outwardly propagating waves in the far field ($K_n(-ikr) \sim \sqrt{\pi/2kr}\, e^{i(kr+\pi/4)}$ for $r \to \infty$) is $\mathcal{A}(\vartheta) = \sum_{n=-\infty}^{\infty} a_n e^{in\vartheta}$, where $a_n = -(\pi/2)\psi_0(0)\tilde{c}_{0,n}$ and $\tilde{c}_{0,n}$ are the components of the scattering wave coefficient vector $\tilde{\boldsymbol{c}} = (\mathbf{I} + \mathbf{H})\mathbf{T}\boldsymbol{d}^I$ for a body in isolation. With these identities, expression (16) reduces to

$$\sigma = \frac{\psi_0^2(0)\pi^2}{k} \sum_{n=-\infty}^{\infty} |\tilde{c}_{0,n}|^2 = \frac{4}{k}\sum_{n=-\infty}^{\infty} |a_n|^2. \quad (17)$$

Since this definition of σ depends on radiated waves in addition to the scattered ones, σ is different for C, F, and X bodies, Fig. 2(b). If we apply the conservation principle for energy carried by incident waves, outwardly propagating waves and energy potentially being extracted by the isolated body, and we use the definitions of σ and the capture width W, we obtain

$$kW + k\sigma = -4\operatorname{Re}\mathcal{A}(\theta_I), \quad (18)$$

which is a generalization of the standard optical theorem for the diffraction problem alone,[21] now applicable to oscillating and energy extracting bodies as well. In all our calculations on isolated bodies, (18) is satisfied to $o(10^{-8})$.

IV. THE EFFECT OF REFLECTORS ON ARRAY GAIN

To analyze the effect of spatial configuration on the array gain, we conduct a series of computations using the multiple scattering model for a range of spatial configuration parameters, incident wavenumbers k and angles θ_I. In this section, we present results for normally incident waves $\theta_I = 0$, which capture the salient physics.

In Sec. IV A, we establish the energy extraction and scattering performance of S-arrays, which we use as a benchmark for comparison and as a basis for explanation of C-R array performance. The energy extraction performance of C-R arrays is presented in Sec. IV B.

A. Performance of S-arrays

The array gain q_S of a single infinitely periodic row of converters was previously studied for optimal point absorbers[13,14] and for finite-sized bodies.[17] We present here the scattering response of S-arrays as a function of periodicity d and body type; we reproduce the q_S results as a basis for comparison with and for the analysis of C-R arrays.

Through coherent wave interactions, the gain q_S of a $\mathcal{S}_C$ array can reach large values ($q_S > 2$), Fig. 4(a). At body-resonant wavenumber k_r, the maximum gain for optimal periodicity is $q_S(k_r) \approx 2$; it is achieved for kd values below the first critical wavenumber $[k_r d < (kd)^{cr}_1]$, Fig. 4(b). Generally, between two critical wavenumbers, $(kd)^{cr}_m$ and $(kd)^{cr}_{m+1}$, the gain q_S increases with kd before abruptly dropping to zero at $(kd)^{cr}_{m+1}$. The obtained values of $q_S(k_r d)$ are lower than maximum[13] $\tilde{q}_S$ since the extraction rate $\beta = \beta^*$ is not optimal in an array setting, resulting in non-optimal motion of WECs. The difference between $q_S(k_r d)$ and $\tilde{q}_S(k_r d)$, however, diminishes with $k_r d$, except for $k_r d$ just under critical wavenumbers $(kd)^{cr}_m$.

The scattering response of an S-array, characterized by the far-field complex amplitudes A^+_m and A^-_m, depends on the scattering cross section σ of the devices and also on the array periodicity d. The amplitudes of the zeroth reflected mode $|A^-_0|$ of $\mathcal{S}_F$, $\mathcal{S}_X$, and $\mathcal{S}_C$ arrays as a function of periodicity d at k_r are shown in Fig. 4(c). While σ for each device is independent of d, $|A^-_0|$ shows great variability. In general, larger σ is correlated with larger achievable values of $|A^-_0|$. Notably, a $\mathcal{S}_F$ array of periodicity $d = d^*_F$ (denoted as $\mathcal{S}^*_F$-array) achieves a perfect reflection of the incident wave at k_r (with $|A^-_0(k_r d^*_F)| \cong 1$), which is significantly stronger than the reflection achieved by $\mathcal{S}_X$ or $\mathcal{S}_C$ arrays at any other non-zero wavenumber. One can conjecture that the

$\mathcal{S}^*_F$-array can significantly affect the performance of a WEC array at k_r if it is used as a reflector row.

B. Performance of C-R arrays

We now analyze the performance of C-R arrays as a function of periodicity d and inter-row spacing d_x. For clarity, we focus on unstaggered C-F arrays of equal periodicity ($d_C = d_R$, row shift $s = 0$), which capture the salient physics of interactions in C-R arrays.

The maximum gain q_F of C-F arrays is significantly larger than that achieved by S-arrays, Fig. 5(a). For example, two C-F array configurations ($d/2a = 3$, $d_x/2a = -2.75$; $d/2a = 6$, $d_x/2a = 4.2$) achieve $q_F \approx 4$ at k_r, Fig. 5(a), compared to $q_S(k_r) < 2$ for $\mathcal{S}_C$ arrays with identical periodicities (cf. Fig. 4). The gain q_F exhibits more extrema than q_S due to the additional wave interactions that occur in C-F arrays.

At k_r, large values of $q_F(k_r) > 4$ are, in fact, achieved by many configurations, Fig. 5(b). Similar to those of $\mathcal{S}_C$ arrays, the peak q_F values correspond to configurations that are closer to $(kd)^{cr}_{m+1}$ than to $(kd)^{cr}_m$. Unlike those of $\mathcal{S}_C$ arrays, though, the peak q_F values do not decrease with kd, indicating the importance of constructive interferences with higher scattered modes ($|m| \geq 1$) in C-R arrays. Although there is a notable asymmetry in the strength of interferences between the C → F and F → C configurations, the maximum values of q_F are comparable. A particularly revealing asymmetry can be observed for $d/2a = 3$ arrays, where C → F configurations exhibit $q_F > 4$ values, while F → C configurations exhibit consistently lower values ($q_F \lesssim 0.5$), Fig. 5(c). The asymmetry is due to the particularly strong reflection from the F-reflector row for this d (identical to $\mathcal{S}^*_F$-array), with $|A^-_0| \approx 1$ [Fig. 4(c)]. This results in high free-surface amplitudes for the well-spaced C → F configurations, and overall low free-surface amplitudes in F → C configurations since $|1 + A^+_0| \approx 0$.

The large values of q are necessarily associated with an increase in WEC motion amplitude. In S-, C-X, and C-F arrays, the motion
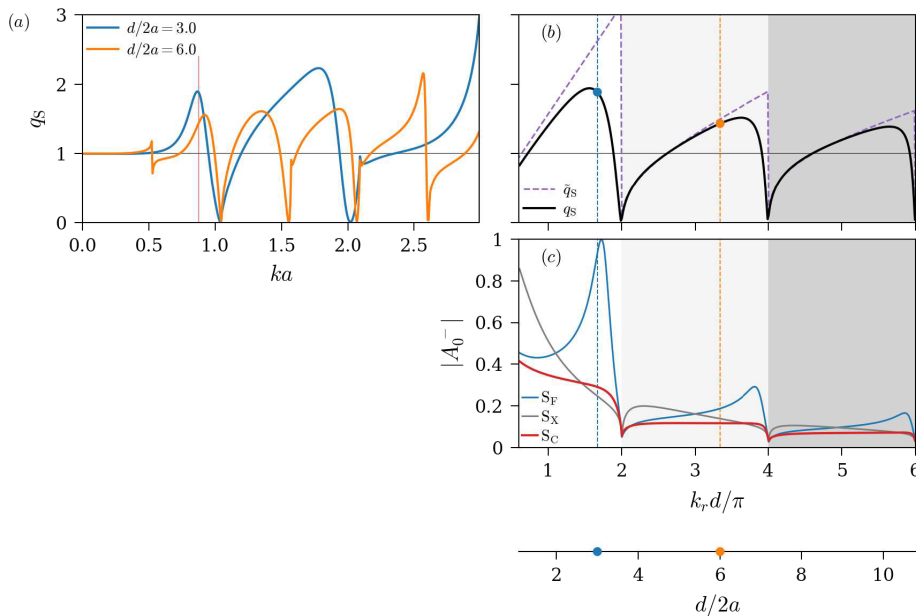
FIG. 4. Single-row periodic array performance (S-array) in normal $\theta_I = 0$ incidence. (a) Array gain q_S of $\mathcal{S}_C$ arrays of two different configurations as a function of wavenumber ka. (b) Array gain q_S at body resonant wavenumber k_r as a function of periodicity d. Array gain of optimal WECs[13] $\tilde{q}_S$ is plotted for comparison. (c) Amplitude of the reflected wave mode $|A^-_0|$ at k_r of $\mathcal{S}_F$, $\mathcal{S}_X$, and $\mathcal{S}_C$ arrays as a function of d.
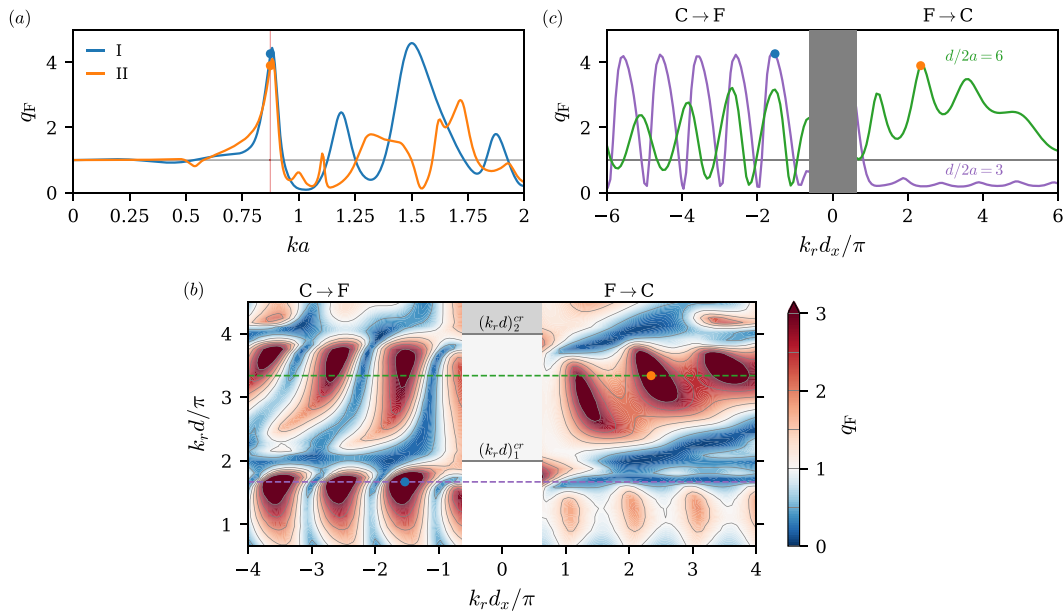
FIG. 5. Performance of C-F arrays. (a) Array gain q_F as a function of wavenumber k for two different configurations (I: $d/2a = 3$, $d_x/2a = -2.75$; II: $d/2a = 6$, $d_x/2a = 4.2$). The values of q_F at body resonant wavenumber k_r are marked with dots of matching color for each configuration. (b) Contour plot of q_F at k_r as a function of periodicity d and inter-row spacing d_x. The configurations I and II are marked with dots in corresponding color. (c) Array gain q_F at k_r as a function of d_x for configurations of two different periodicities d.

amplitudes of WECs are $\sqrt{q}$ times larger than that of isolated WECs. As a result, the assumptions of linear wave-body interactions are stretched or violated at these instances and the nonlinear effects can become significant. However, even though the achieved values of q might need correction due to the nonlinear effects, the linear results presented here for the conditions that lead to high q values (and, consequently, the array configurations for which they occur) likely hold.

V. A PHYSICAL ARGUMENT FOR THE PRESENCE AND LOCATION OF EXTREMA IN THE ARRAY GAIN

The areas corresponding to C-R array configurations of high q-values, Fig. 5(b), are criss-crossed by regions where q is significantly lower. To elucidate these features in the q-values, we present a simple physical argument based on the constructive and destructive interferences in the C-R arrays. We build the argument from a plane wave interaction model based on the far-field response of S-arrays.

Consider a wavefield, far away from an S-array, that consists of the superposed incident wave propagating at θ_I and a single scattered plane wave mode of amplitude $A_m^\pm$. The resulting wave envelope is an undulating surface, generally periodic in both normal and span-wise directions. A periodic row of converters, configured in such a way that the position of each converter corresponds to a wave envelope peak, should result in maximum energy extraction. Conversely, if the position of each converter corresponds to a wave envelope trough, the energy extraction is minimized. The locations of these envelope peaks and troughs depend on the phase differences between interacting plane waves, which can be determined from S-arrays alone and depend on the array periodicity d. This implies that no near-field interactions exist among the rows and that at most a single reflection occurs at the reflector row. We are primarily interested here in

determining the configuration conditions that lead to the extrema of gain, which are less affected by these assumptions.

Consider a wave incident at a C $\rightarrow$ R array, propagating in the θ_I direction with $kd < (kd)_1^{cr}$. The interaction between the incident wave and the wave reflected from the R-row and propagating at $\pi - \theta_I$, Fig. 6, results in an undulating free surface envelope whose generatrix is a straight line parallel to the reflecting structure. We refer to this interaction as Bragg interference. The minima of the envelope (i.e., destructive Bragg interferences) are located at

$$kd_x \cos\theta_I = n\pi + \delta^B/2, \quad n \in \mathbb{Z}, \tag{19}$$

where δ^B is the periodicity-dependent phase function. Here, $\delta^B(d) = \arg(A_{0,R}^-(1 + A_{0,C}^+))$ stems from the phase shifts of the transmitted wave occurring at the C-row and of the reflected wave at the R-row. The additional subscript to $A_m^\pm$ refers to the row (C or R) at which the phase shift occurs. Constructive interference, resulting in maximum q for a particular d, occurs for $\delta^B + \pi$. While (19) could explain the Bragg-like features in R $\rightarrow$ C arrays, the single-scattering model does not technically apply for those configurations as there is no reflected wave, to leading order, at the C-row with which the incident wave can interfere.

The interaction between an incident wave and a higher scattered mode $A_m^\pm$, $|m| \geq 1$, leads to an undulating wave envelope that is periodic in the span-wise direction. When occurring in array configurations in which the converters are located at the extrema of the wave envelope, we refer to these interactions as Laue interferences.[17] The minima of the envelope resulting from destructive Laue interferences between the incident wave and the mth mode occur at

$$kd_x(\cos\theta_I - \cos\theta_m) = 2n\pi + \delta_m^L, \quad n \in \mathbb{Z}. \tag{20}$$
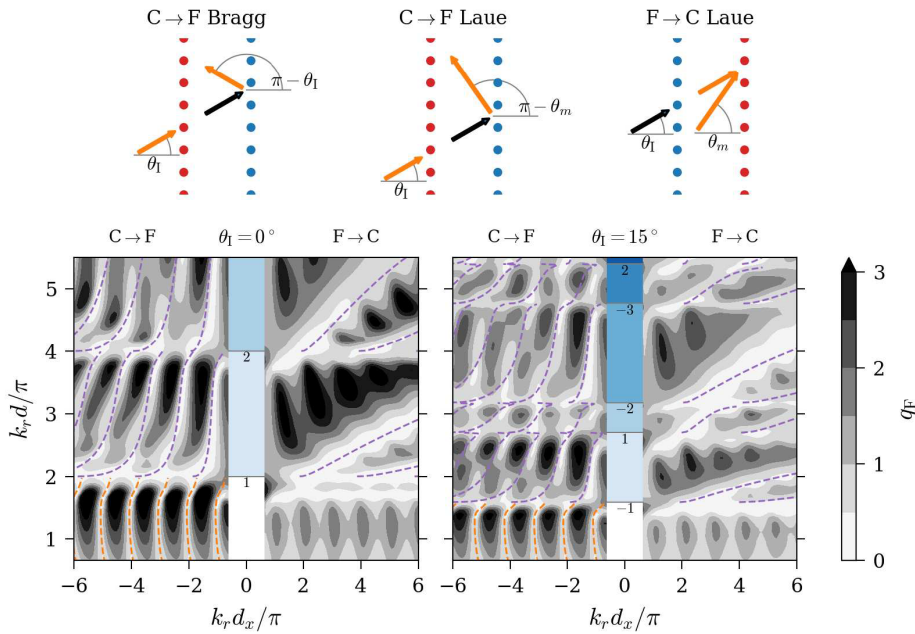
FIG. 6. Single-scattering predictions of Bragg and Laue interferences in C-F arrays. Top: Sketches of the interference mechanisms. Wavevectors of the interacting plane waves are depicted in orange. Bottom: Interference lines (ILs) of destructive Bragg (orange lines) and Laue (purple lines) interferences for waves incident at $\theta_I = 0°$ and $15°$.

The phase shift δ_m^L of mode m depends on the array configuration and on periodicity d. For C $\rightarrow$ R configurations, $\delta_m^L(d) = \arg(A_{m,R}^-(1 + A_{0,C}^+))$; for R $\rightarrow$ C configurations, $\delta_m^L(d) = \arg(A_{m,R}^+(1 + A_{0,R}^+))$. Constructive Laue interferences occur at $\delta_m^L + \pi$ and correspond to the maxima of the wave envelope.

The conditions (19) and (20) in d–d_x space result in a family of interference lines (ILs) corresponding to the destructive Bragg and Laue interferences. In C-F arrays, these ILs predict well the minima of gain q_F obtained through multiple-scattering simulations, Fig. 6. (For clarity, the ILs are drawn only in kd-ranges in which they first appear; technically they extend for $kd \rightarrow \infty$ values. As the amplitude of the plane modes diminishes with kd, the interactions are the strongest in the first kd range.) The maxima of q_F contained between the drawn destructive ILs lie near the constructive ILs (not drawn). While the conditions for Bragg and Laue interferences are determined by the array configuration and the phase shift at the scattering structure, their strength is governed by the amplitudes of the interacting modes. As such, Bragg and Laue interferences are less noticeable when the interfering scattered modes are not strong. Furthermore, this model applies only to the first-order interactions; the fringes in q_F that are not explained by the drawn ILs are due to the higher-order interactions. For example, the Bragg interferences, which are pronounced C $\rightarrow$ F arrays, exist in F $\rightarrow$ C arrays as well, although much less pronounced due to the absence of the interaction between the first-order reflected and incident waves.

VI. THE OPTIMAL PERFORMANCE OF GENERAL C-R ARRAYS

So far, we have focused on canonical C-R array configurations ($d_C = d_R$, row shift $s = 0$, reflector periodicity factor $\nu = 1$) to elucidate the salient physics governing their behavior. We now also consider generalized C-R array configurations ($d_C \neq d_R$, $s \neq 0$, and R = F, X, or C) and present quantitative comparisons between the

optimal configurations for a range of incident angles θ_I at body resonant k_r. We present results for $\theta_I \in [0°, 75°]$; the energy extracted by a periodic array for $\theta_I = 90°$ drops to zero. With this θ_I range, we also capture the behavior of C-R arrays for $\theta_I > 90°$ by considering both C $\rightarrow$ R and R $\rightarrow$ C arrays; the behavior of C-R arrays for $-\theta_I$ is captured by considering symmetric values of row shift s around zero. For every θ_I, we define q^* as the maximal value of gain at k_r achieved over all possible spatial configurations (in d– or d–d_x space) considered. For clarity, we assign subscripts to q^* to differentiate between the array configuration considered—R (= F, X, C) or $\mathcal{S}$. The main interest for the present problem, finally, is how q_R^* compares with $q_{\mathcal{S}}^*$.

The optimal canonical C-R arrays ($s = 0$, $\nu = 1$), as a result of favorable wave interactions with the reflector row, achieve higher optimal gain q_R^* over the optimal gain $q_{\mathcal{S}}^*$ of $\mathcal{S}_C$-arrays for all θ_I, Fig. 7(a). C-F arrays are particularly effective as they achieve $q_F^* = 4.94$ for $\theta_I = 0$. The resulting gain due to the reflectors is $Q_R \equiv q_F^*/q_{\mathcal{S}}^* \approx 2.5$, which is achieved in addition to the maximum array gain of the optimal $\mathcal{S}_C$ array. Note that here the comparison is being made between the *optimal* configurations, which generally do not have identical periodicity d. Remarkably, for the device shape we study here, the total energy extracted by the optimal C-F array ($N_C = 1$) in normal incidence is greater than the energy extracted by the optimal C-C arrays, which consists of twice as many converters ($N_C = 2$), Fig. 7(a). (In order to compare the absolute extracted power P of C-C arrays with that of other C-R arrays in Fig. 7(a), we compare q_R^* to $2 \times q_C^*$ since q_C^* is normalized by $N_C = 2$.) This indicates that adding reflectors to a WEC array *could* lead to greater energy extraction than adding additional converters would. Generally, q^* decreases with increasing θ_I for all array configurations, consistent with the behavior of periodic WEC arrays[17] and WEC arrays with randomized spatial configurations.[31,32]

In general, a higher gain q_R^* is achieved for reflectors with a larger total scattering cross section σ. For example, q_F^* is significantly greater than q_X^* for all θ_I at k_r [Fig. 7(a)] since σ of F-reflectors is significantly
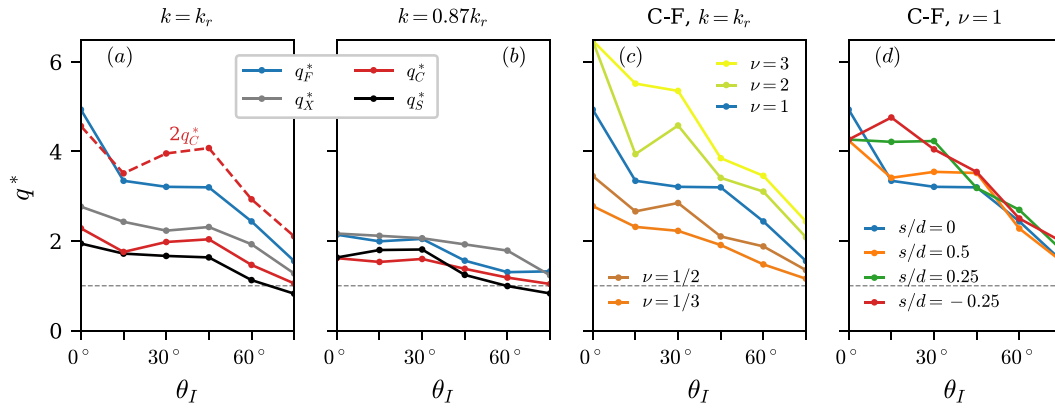
FIG. 7. The maximum gain q^* as a function of incident angle θ_I. Comparison of C-R arrays of different reflector types ($d_C = d_R$, $s = 0$, $\nu = 1$) at (a) $k = k_r$ and (b) $k = 0.87k_r$. (c) The effect of reflector periodicity factor ν on q_F^* of C-F arrays ($s = 0$) at k_r. (d) The effect of row shift s on q_F^* of C-F arrays ($\nu = 1$) at k_r.

greater than that of X-reflectors [Fig. 2(b)]. Since we consider here the optimal q^* values, the periodicity dependence of $|A_0^-|$ is not relevant because the maximum $|A_0^-|$ values are correlated with σ. For wavenumbers where σ of F- and X-reflectors are comparable, the resulting optimal gains q_F^* and q_X^* are comparable as well; this is exemplified in Fig. 7(b) for $k = 0.87\,k_r$ at which $\sigma_F = 0.85\,\sigma_X$ [Fig. 2(b)].

The optimal gain q_R^* can be further increased by increasing the scattering from the reflectors per WEC. Without altering the reflector geometry, the scattering strength can be modified by changing the periodicity d_R of the reflectors, i.e., by changing the reflector periodicity factor ν. We consider here $\nu \in \{1/3, 1/2, 1, 2, 3\}$, Fig. 7(c). Doubling the number of reflectors per WEC ($\nu = 2$) increases the optimal gain to $q_F^* \approx 6.5$ for normal incidence. A further increase to $\nu = 3$ does not improve q_F^* at $\theta_I = 0$, but it does improve it for other incidence angles. Conversely, $\nu < 1$, i.e., a lower σ per cell, results in consistently lower q_F^* values.

Introducing a non-zero shift s between the two rows does not improve the performance of C-R arrays in normal incidence, Fig. 7(d). For intermediate $15° \lesssim \theta_I \lesssim 45°$ incidence, staggered ($s \neq 0$) C-F arrays achieve larger q_F^*, but not as much as those with increased reflector scattering (e.g., for $\nu = 3$). The qualitatively similar results for varying s values indicate the robustness of gain enhancement in C-R arrays.

The performance of C-R arrays in irregular seas is obtained by integrating the array gain over the wave spectrum and possible directional spread. For very narrow-banded spectra with peak wavenumber k_p, the optimal spectral array gain is similar to $q_R^*(k_p)$, but with the increase in spectrum bandwidth, the optimal spectral array gain will decrease. Due to the strength of constructive interferences and the associated gain, the optimal C-R array configuration in irregular seas is likely to be close to the optimal one for monochromatic seas at k_p. In directional seas (directional wave spreading function $f(\theta)$, $\int_{2\pi} f\, d\theta = 1$), the directionally averaged gain $\langle q \rangle$ decreases as the spread increases, with the upper bound[31]

$$\langle q \rangle = \int_{2\pi} q(\theta)f(\theta)\, d\theta \leq \frac{2\pi}{kW} \max_\theta f . \tag{21}$$

For isotropic incidence ($f = 1/2\pi$) on an array of optimally heaving WECs, (21) simplifies to an equality $\langle q \rangle = 1$;[31,33,34] in unidirectional seas ($f = \delta(\theta - \theta_I)$, with δ being the Dirac delta function), $\langle q \rangle = q(\theta_I)$

is recovered. For practical purposes, the maximum deviation of the incident angle from the mean wave direction on an infinitely periodic array (or a large, but finite array near a shoreline) is significantly narrower ($|\theta| < 90°$), with f being strongly peaked around the mean wave direction (such as in the commonly applicable cosine-$2s$ distribution[35]), so the upper bound on $\langle q \rangle$ is less restrictive.

VII. CONCLUSION

We investigate how the energy extraction of WEC arrays can be increased by harnessing wave reflections from non-extracting reflectors in their vicinity. For C-R arrays, periodic arrays with a row of WECs parallel to a row of axisymmetric reflectors, we find that significant energy extraction gains are achieved when (i) the total scattering cross section σ of the reflectors is large, (ii) the periodicity d is such that the amplitude of the reflected modes is maximized, and (iii) the spacing between the rows is such that the extraction is maximized by utilizing the constructive Bragg or Laue interference. For R → C arrays in particular, the conditions (i) and (ii) are modified in favor of maximizing transmitted modes, and the condition (iii) is primarily valid for the constructive Laue interference.

For converter and reflector characteristics considered here, the C-F array of optimal configuration achieves a gain of $q_F^* \approx 5$ for the resonant wavenumber at normal incidence, which is roughly 2.5 times greater than that of the optimal single-row WEC array. More remarkably, that particular C-F array extracts more energy than the optimal C-C array, even though C-C arrays have twice as many converters.

While the quantitative values presented here are for the specific body shape and PTO values we studied, the potential for large gain increases in C-R arrays remains even if the WEC or the reflector geometry, or the PTO are modified, as long as the scattering from reflectors is strong. Furthermore, while we only considered here a single row of converters parallel to a single row of reflectors, one can conjecture that reflectors can lead to a significant increase in energy extraction in hybrid arrays of more complex spatial configurations as well. Finally, the results presented here are strictly valid for linear wave–body interactions. The achieved large values of gain associated with optimal configurations might be affected when the nonlinear effects and viscosity are taken into account, but the wave interaction mechanisms that occur in these configurations likely hold.

20 November 2023 20:14:23

Our analysis has practical implications for the design and array gains of WEC arrays that might be placed in the vicinity of existing large offshore structures (whether natural or man-made). A special case, for example, is an array of offshore wind turbine supporting structures, which may be similar to what we considered. Even for WEC arrays in isolation, the present results suggest the remarkable possibility of cost reduction and increased energy extraction by replacing select converters with (cheaper) non-extracting reflectors.

ACKNOWLEDGMENTS

AUTHOR DECLARATIONS
Conflict of Interest

The authors have no conflicts to disclose.

Author Contributions

Grgur Tokić: Conceptualization (equal); Formal analysis (lead); Investigation (lead); Methodology (lead); Software (lead); Validation (lead); Visualization (lead); Writing – original draft (lead); Writing – review & editing (equal). **Dick K. P. Yue:** Conceptualization (equal); Funding acquisition (lead); Writing – review & editing (equal).

DATA AVAILABILITY

The data that support the findings of this study are available from the corresponding author upon reasonable request.

APPENDIX: CALCULATION OF LATTICE SUMS

The infinite sum appearing in (10) captures the contributions from the infinite number of bodies in a periodic array. For evanescent waves ($m > 0$), the sum converges quickly and can be summed directly, but the sum is notoriously slowly convergent for propagating wave $m = 0$ solutions[36,37] and it needs a special treatment.

We can express an element $Q_{0,n,l}^{jp}$ of the periodicity matrix defined in (10) as

$$(-1)^l Q_{0,n,l}^{jp} = \sum_{\substack{B = -\infty, \\ B \neq 0}}^{\infty} \mathcal{Q}_{\mu,B} \quad (A1)$$

with $\mu \equiv n - l$. For large $|B| \to \infty$, $R_{jp} \to d|B|$ and $\alpha_{jp} \to \alpha_B = \mp \pi/2$ for $B \gtrless 0$, resulting in the limit

$$\lim_{|B| \to \infty} \mathcal{Q}_{\mu,B} = P_B K_\mu(k_0 d|B|) e^{i\mu\alpha_B} = \mathcal{Q}_{\mu,B}^{\mathcal{S}}, \quad (A2)$$

where $P_B = e^{ikd \sin \theta_I}$. We can now use Kummer's transformation[36] of the original series

$$(-1)^l Q_{0,n,l}^{jp} = \sum_{\substack{B = -\infty, \\ B \neq 0}}^{\infty} \mathcal{Q}_{\mu,B}^{\mathcal{S}} + \sum_{\substack{B = -\infty, \\ B \neq 0}}^{\infty} \left(\mathcal{Q}_{\mu,B} - \mathcal{Q}_{\mu,B}^{\mathcal{S}} \right)$$

$$= (-i)^\mu \sigma_\mu + Q_\mu, \quad (A3)$$

where

$$\sigma_\mu(kd, \theta_I) = i^\mu \sum_{\substack{B = -\infty, \\ B \neq 0}}^{\infty} \mathcal{Q}_{\mu,B}^{\mathcal{S}} = \sum_{B=1}^{\infty} \left[P_B + (-1)^\mu P_{-B} \right] K_\mu(k_0 d|B|) \quad (A4)$$

is the standard Schlömilch sum, for which rapidly convergent formulations are known.[36] With this transformation, the infinite sum in the off-axis correction Q_μ term now converges more rapidly.

The Schlömilch sum σ_μ depends only on the periodicity and not on the relative positions of the body in a periodic cell, so it can be used for many configurations. For the case when the infinite sum is for bodies along the same axis (i.e., $R_{jp} = 0$), $(-1)^l Q_{0,n,l}^{jp} = (-i)^\mu \sigma_{n-l}$.

REFERENCES

[1] A. Babarit, "On the park effect in arrays of oscillating wave energy converters," Renewable Energy **58**, 68 (2013).

[2] M. Göteman, M. Giassi, J. Engström, and J. Isberg, "Advances and challenges in wave energy park optimization—A review," Front. Energy Res. **8**, 26 (2020).

[3] C. Pérez-Collazo, D. Greaves, and G. Iglesias, "A review of combined wave and offshore wind energy," Renewable Sustainable Energy Rev. **42**, 141 (2015).

[4] S. Astariz and G. Iglesias, "Co-located wind and wave energy farms: Uniformly distributed arrays," Energy **113**, 497 (2016).

[5] E. Yablonovitch, "Statistical ray optics," J. Opt. Soc. Am. **72**, 899 (1982).

[6] Z. Yu, A. Raman, and S. Fan, "Fundamental limit of nanophotonic light trapping in solar cells," Proc. Natl. Acad. Sci. **107**, 17491 (2010).

[7] D. N. Konispoliatis and S. A. Mavrakos, "Wave power absorption by arrays of wave energy converters in front of a vertical breakwater: A theoretical study," Energies **13**, 1985 (2020).

[8] E. Loukogeorgaki, C. Michailides, G. Lavidas, and I. K. Chatjigeorgiou, "Layout optimization of heaving Wave Energy Converters linear arrays in front of a vertical wall," Renewable Energy **179**, 189 (2021).

[9] C. M. Linton and D. V. Evans, "The radiation and scattering of surface waves by a vertical circular cylinder in a channel," Philos. Trans. R. Soc. London, Ser. A **338**, 325 (1992).

[10] M. A. Peter, M. H. Meylan, and C. M. Linton, "Water-wave scattering by a periodic array of arbitrary bodies," J. Fluid Mech. **548**, 237 (2006).

[11] L. G. Bennetts and V. A. Squire, "Wave scattering by multiple rows of circular ice floes," J. Fluid Mech. **639**, 213 (2009).

[12] Y. Li and C. C. Mei, "Bragg scattering by a line array of small cylinders in a waveguide. Part 1. Linear aspects," J. Fluid Mech. **583**, 161 (2007).

[13] M. A. Srokosz, "Some relations for bodies in a canal, with an application to wave-power absorption," J. Fluid Mech. **99**, 145 (1980).

[14] J. Falnes and K. Budal, "Wave-power absorption by parallel rows of interacting oscillating bodies," Appl. Ocean Res. **4**, 194 (1982).

[15] X. Garnaud and C. C. Mei, "Bragg scattering and wave-power extraction by an array of small buoys," Proc. R. Soc. A **466**, 79 (2010).

[16] E. Renzi and F. Dias, "Resonant behaviour of an oscillating wave energy converter in a channel," J. Fluid Mech. **701**, 482 (2012).

[17] G. Tokić and D. K. P. Yue, "Hydrodynamics of periodic wave energy converter arrays," J. Fluid Mech. **862**, 34 (2019).

[18] S. Zheng, Y. Zhang, and G. Iglesias, "Wave–structure interaction in hybrid wave farms," J. Fluids Struct. **83**, 386 (2018).

[19] C. C. Mei, "Hydrodynamic principles of wave power extraction," Philos. Trans. R. Soc., A **370**, 208 (2012).

[20] R. G. Newton, *Scattering Theory of Waves and Particles* (Springer Berlin Heidelberg, 1982).

[21] C. C. Mei, M. S. Stiassnie, and D. K. P. Yue, "Theory and applications of ocean surface waves," in *Advanced Series on Ocean Engineering* (World Scientific, 2005).

[22] R. Porter, S. Zheng, and H. Liang, "Scattering of surface waves by a vertical truncated structured cylinder," Proc. R. Soc. A **478**, 20210824 (2022).

[23]H. Kagemoto and D. K. P. Yue, "Interactions among multiple three-dimensional bodies in water waves: An exact algebraic method," J. Fluid Mech. **166**, 189 (1986).

[24]M. Abramowitz and I. A. Stegun, *Handbook of Mathematical Functions: With Formulas, Graphs, and Mathematical Tables* (Courier Corporation, 1964), Vol. 55.

[25]R. W. Yeung, "Added mass and damping of a vertical cylinder in finite-depth waters," Appl. Ocean Res. **3**, 119 (1981).

[26]C. J. R. Garrett, "Wave forces on a circular dock," J. Fluid Mech. **46**, 129 (1971).

[27]P. A. Martin, *Multiple Scattering*, Encyclopedia of Mathematics and its Applications (Cambridge University Press, Cambridge, 2006).

[28]Lord Rayleigh, "On the dynamical theory of gratings," Proc. R. Soc. London, Ser. A **79**, 399 (1907).

[29]A. Hessel and A. A. Oliner, "A new theory of Wood's anomalies on optical gratings," Appl. Opt. **4**, 1275 (1965).

[30]C. M. Linton and I. Thompson, "Resonant effects in scattering by periodic arrays," Wave Motion **44**, 165 (2007).

[31]M. Benzaouia, G. Tokić, O. D. Miller, D. K. P. Yue, and S. G. Johnson, "From solar cells to ocean buoys: Wide-bandwidth limits to absorption by metaparticle arrays," Phys. Rev. Appl. **11**, 034033 (2019).

[32]G. Tokić and D. K. Yue, "Hydrodynamics of large wave energy converter arrays with random configuration variations," J. Fluid Mech. **923**, R1 (2021).

[33]C. Fitzgerald and G. Thomas, in *Proceedings of the 7th European Wave and Tidal Energy Conference* (European Wave and Tidal Energy Conference, 2007).

[34]H. A. Wolgamot, P. H. Taylor, and R. Eatock Taylor, "The interaction factor and directionality in wave energy arrays," Ocean Eng. **47**, 65 (2012).

[35]M. K. Ochi, *Ocean Waves* (Cambridge University Press, 1998).

[36]C. M. Linton, "The Green's function for the two-dimensional Helmholtz equation in periodic domains," J. Eng. Math. **33**, 377 (1998).

[37]C. M. Linton, "Schlömilch series that arise in diffraction theory and their efficient computation," J. Phys. A **39**, 3325 (2006).

20 November 2023 20:14:23